

GAMMA-RAY LUMINOSITY FUNCTION OF BLAZARS AND THE COSMIC GAMMA-RAY BACKGROUND: EVIDENCE FOR THE LUMINOSITY DEPENDENT DENSITY EVOLUTION

TAKURO NARUMOTO AND TOMONORI TOTANI

Department of Astronomy, School of Science, Kyoto University, Sakyo-ku, Kyoto, 606-8502, Japan

Accepted for Publication in The Astrophysical Journal

ABSTRACT

We present a comprehensive study for the gamma-ray luminosity function (GLF) of blazars and their contribution to the extragalactic diffuse gamma-ray background (EGRB). Radio and gamma-ray luminosity correlation is introduced with a modest dispersion consistent with observations, to take into account the radio detectability which is important for the blazar identification. Previous studies considered only pure luminosity evolution (PLE) or pure density evolution, but here we introduce the luminosity dependent density evolution (LDDE) model, which is favored from the evolution of X-ray luminosity function (XLF) of AGNs. The model parameters are constrained by likelihood analyses about the observed redshift and gamma-ray flux distributions of the EGRET blazars. Interestingly, we find that the LDDE model gives a better fit to the observed distributions than the PLE model, indicating that the LDDE model is also appropriate for gamma-ray blazars, and that the jet activity is universally correlated with the accretion history of AGNs. The normalization between the GLF and XLF is consistent with the unified picture of AGNs, when the beaming and a reasonable duty cycle of jet activity are taken into account. We then find that only 25–50% of the EGRB can be explained by unresolved blazars with the best-fit LDDE parameters. Unresolved blazars can account for all the EGRB only with a steeper index of the faint-end slope of the GLF, which is marginally consistent with the EGRET data but inconsistent with that of the XLF. Therefore unresolved AGNs cannot be the dominant source of the EGRB, unless there is a new population of gamma-ray emitting AGNs that evolves differently from the XLF of AGNs. Predictions for the *GLAST* mission are made, and we find that the best-fit LDDE model predicts about 3000 blazars in the entire sky, which is considerably fewer (by a factor of more than three) than a previous estimate.

Subject headings: diffuse radiation — galaxies: active — galaxies: evolution — galaxies: luminosity function — gamma rays: theory — quasars: general

1. INTRODUCTION

The origin of the extragalactic diffuse gamma-ray background (EGRB) is one of the unsolved problems in astrophysics. The EGRB was first discovered by the *SAS* 2 satellite (Fichtel, Simpson, & Thompson 1978; Thompson & Fichtel 1982) and subsequently confirmed by the Energetic Gamma Ray Experiment Telescope (EGRET) instrument aboard the *Compton Gamma Ray Observatory* (*CGRO*). In the first analysis of the EGRET data, the flux of the EGRB integrated above 100 MeV was determined to be $(1.45 \pm 0.05) \times 10^{-5}$ photons $\text{cm}^{-2} \text{s}^{-1} \text{sr}^{-1}$ (Sreekumar et al. 1998). However, this value is strongly dependent on the modeling of the Galactic background, which is dominated by cosmic-ray interactions in the Galactic disk and must be subtracted from the background data. The latest analysis, which used a new model of the Galactic background, resulted in a slightly smaller value of the EGRB, $(1.14 \pm 0.12) \times 10^{-5}$ photons $\text{cm}^{-2} \text{s}^{-1} \text{sr}^{-1}$ (Strong et al. 2004).

EGRET detected many extragalactic high-energy gamma-ray sources that have been identified as active galactic nuclei (AGNs). Most of them fall into the blazar class of AGNs, and this is the only one extragalactic population confirmed in the third EGRET catalog (Hartman et al. 1999), constituting about 15% of the EGRB flux. Therefore unresolved blazars are the most likely candidate for the origin of the EGRB, at least contributing substantially, and this issue has been studied in a number of papers (Padovani et al. 1993; Stecker, Salamon, & Malkan 1993; Salamon & Stecker 1994; Chiang et al. 1995; Stecker & Salamon 1996; Chiang & Mukherjee

1998; Mücke & Pohl 2000). On the other hand, several alternative candidates for the EGRB components have been proposed, e.g., intergalactic shocks produced by the formation of large-scale cosmological structures (Loeb & Waxman 2000; Totani & Kitayama 2000; Miniati 2002; Scharf & Mukherjee 2002; Gabici & Blasi 2003; Keshet et al. 2003), or dark matter annihilation (Oda, Totani, & Nagashima 2005 and references therein). Therefore, it is important to determine whether the number of unresolved blazars are enough to account for all of the EGRB, but conclusions derived by the earlier studies are somewhat controversial.

Stecker & Salamon (1996, hereafter SS96) estimated the unresolved blazar contribution with basic assumptions that EGRET blazars are the same population with flat-spectrum radio-loud quasars (FSRQs), and that the gamma-ray and radio luminosities are linearly related. Then they constructed the blazar gamma-ray luminosity function (GLF) model from the FSRQ radio luminosity function (RLF), and found that blazars can account for 100% of the EGRB. However, their model was not compared with the available redshift distribution of the EGRET blazars, and hence it was uncertain whether this GLF model is statistically consistent with the EGRET blazar data.

Quantitative comparison of GLF models to the flux and redshift distributions of the EGRET blazars was performed by Chiang & Mukherjee (1998, hereafter CM98), and indeed, they found that the model of SS96 seriously overpredicts the number of low-redshift blazars detectable by the EGRET. CM98 then concluded that blazars can account for only 25% of the EGRB, based on the GLF model consistent with the

EGRET blazar distributions.¹

However, the analysis of the GLF is not straightforward; a source of uncertainty is the detectability in the radio band. Most of the EGRET blazars are identified by finding radio counterparts, and hence they would remain unidentified if their radio counterparts are under the flux limit of radio surveys, even though their gamma-ray flux is above the EGRET sensitivity limit. Therefore one must estimate the probability of a model blazar having flux greater than the sensitivity limits, not only in the gamma-ray band but also in the radio band. CM98 introduced this probability in their analysis, but they assumed that there is no correlation between gamma-ray and radio luminosities of blazars. However, the assumption of no correlation at all over a wide range of gamma-ray and radio luminosities induces some inconsistencies (see discussion given in Stecker & Salamon 2001), and it is physically reasonable to expect some level of correlation from the viewpoint of the standard synchrotron-inverse Compton model of blazars. Therefore we adopt a new treatment on this issue introducing a reasonable correlation (see §2.3 for details).

Mücke & Pohl (2000) approached this issue from the viewpoint of the unification scheme of radio-loud AGNs, which proposed that blazars are the beamed subclass of Fanaroff-Riley (FR) radio galaxies. They considered the GLF models based on the RLF of FR galaxies, and the flux and redshift distributions of blazars were used to constrain their GLF models. Then they concluded that unresolved blazar contribution to the EGRB is 20–40% assuming that the blazars extend to the maximum cutoff redshift of $z_{\text{max}} = 3$, and 40–80% for $z_{\text{max}} = 5$. However, the identification probability of a blazar, which may affect the estimate of the blazar contribution to the EGRB, was not incorporated in their analysis.

To resolve this rather controversial situation, in this paper we make a comprehensive study of GLF models that are statistically compared with the observed redshift and flux distributions, taking into account a reasonable correlation between gamma-ray and radio flux in a consistent manner with the observed gamma-ray to radio flux ratios. Then we make an estimate of the blazar contribution to the EGRB flux, and also estimate the expected number of “unidentified blazars” due to the lack of radio detection, which can be compared with the number of high-Galactic-latitude unidentified sources in the third EGRET catalog. We also make some predictions for the future *Gamma Ray Large Area Space Telescope* (GLAST) observation, and discuss its prospects.

In addition to these new aspects, we also try a new type of the GLF evolution model. The earlier studies treated the cosmological evolution of the blazar GLF as a pure luminosity evolution (PLE) or a pure density evolution. On the other hand, the cosmological evolution of the luminosity function of AGNs has been investigated intensively in soft X-ray (e.g., Miyaji, Hasinger, & Schmidt 2000, 2001; Hasinger, Miyaji, & Schmidt 2005) and hard X-ray (e.g., Boyle et al. 1998; La Franca et al. 2002; Cowie et al. 2003; Ueda et al. 2003) bands, recently. The former studies are mostly for type 1 AGNs, while the latter ones are for both type 1 and 2 AGNs, since soft X-ray emission of type 2 AGNs is significantly absorbed. These studies revealed that the overall behavior of the soft X-ray luminosity function (SXLf) and hard X-ray

luminosity function (HXLf) of AGNs are very similar and best described with a luminosity dependent density evolution (LDDE) where the peak redshift of density evolution increases with AGN luminosity (Miyaji, Hasinger, & Schmidt 2000, 2001; Ueda et al. 2003; Hasinger, Miyaji, & Schmidt 2005). Therefore it is reasonable to expect that the cosmological evolution of the blazar GLF may also be expressed by the LDDE. In this paper, we try two kinds of blazar GLF model; one is based on the FSRQ RLF (PLE model) and the other is based on the AGN SXLf (LDDE model).

The paper will be organized as follows: In §2, we describe sample definition and formulations for the statistical analyses. In §3, we present models of the blazar GLF and results of comparison to the EGRET data. In §4, we address the prospects for the *GLAST* mission. Discussions and conclusions are given in §5 and §6, respectively. Throughout this paper, we adopt a Λ CDM universe with the density parameter $\Omega_0 = 0.3$, the cosmological constant $\Omega_\Lambda = 0.7$, and the Hubble constant $H_0 = 70 \text{ km s}^{-1} \text{ Mpc}^{-3}$.

2. FORMULATIONS

2.1. Sample Definition

Most of blazars show considerable variability, but it is difficult to incorporate in the statistical analysis of the GLF. Therefore we use the mean flux shown in the third EGRET catalog. There are some blazars in the EGRET catalog whose significance of detection is above the EGRET threshold (4σ for $|b| > 10^\circ$, and 5σ for $|b| < 10^\circ$) only in some viewing periods, and their mean significance of detection is under the EGRET threshold. We exclude such blazars from our analysis, and use only blazars whose mean significance of detection (as shown in the catalog) is above the EGRET threshold. There are 46 blazars meeting this selection.

Since the detection limit is sensitively dependent on the location in the sky, we will take it into account in the analysis. In the left panel of Figure 1 we plot the EGRET detection limit for each EGRET point source, which is calculated from mean flux and mean statistical significance of the detection by using equation (1) of CM98, against its Galactic latitude (*crosses*). The best-fit relation is also shown (*solid line*). Because of the variability, this fit may be different from the effective detection threshold for blazars that we have chosen. In order to check this point, in the right panel of Figure 1 we plot the mean flux of the EGRET blazars, comparing them to the obtained detection limit curve. We see from this figure that most of blazars are above the detection limit curve, and hence it is reasonable to take this curve as the EGRET detection limit for the 46 blazars used in this paper.

It is difficult to take into account the variety of blazar spectra, and we assume a single universal power-law spectrum for all blazars, with the photon spectral index of $\alpha = 2.2$ ($dN_\gamma/dE_\gamma \propto E_\gamma^{-\alpha}$). This value is close to the mean of the EGRET blazars ($\alpha = 2.15 \pm 0.04$, Sreekumar et al. 1998). We confirmed that our conclusions in this paper are not seriously affected even if we change the value of this parameter into $\alpha = 2.1$ and 2.3. Then, the gamma-ray luminosity L_γ , which is defined as νL_ν in erg s^{-1} at 100 MeV (at the restframe), is related to the observed photon flux, F_γ at $E_\gamma \geq E_{\text{min}} \equiv 100 \text{ MeV}$ (in photons $\text{cm}^{-2} \text{ s}^{-1}$ and E_{min} in the observer’s frame), as

$$L_\gamma = 4\pi d_L^2 \frac{\alpha - 1}{(1+z)^{2-\alpha}} E_{\text{min}} F_\gamma, \quad (1)$$

where d_L is the standard luminosity distance. Then, the ob-

¹ In this paper, we refer the fraction of the blazar contribution in the EGRB always removing the already detected EGRET blazars, i.e., the ratio of the background flux from blazars under the EGRET detection limit to the EGRB flux of $1.14 \times 10^{-5} \text{ photons cm}^{-2} \text{ s}^{-1}$ reported by Strong et al. (2004).

served data that will be used in the statistical analysis is a set of $(z_i, L_{\gamma,i}, \Omega_i)$, where Ω_i denotes the observed blazar location in the sky, and the subscript i denotes each blazar, running over $1 \leq i \leq N_{\text{obs}} = 46$.

2.2. Maximum Likelihood Method

We constrain the model parameters of the blazar GLF models by using the maximum likelihood method. A specified GLF model predicts the distribution function of the three quantities, $d^3N/(dz dL_{\gamma} d\Omega)$, and the likelihood function \mathcal{L} is given as (see, e.g., Lored & Lamb 1989):

$$\mathcal{L} = \exp(-N_{\text{exp}}) \prod_{i=1}^{N_{\text{obs}}} \frac{d^3N(z_i, L_{\gamma,i}, \Omega_i)}{dz dL_{\gamma} d\Omega}, \quad (2)$$

where N_{exp} is the expected number of blazar detections:

$$N_{\text{exp}} = \int dz \int dL_{\gamma} \int d\Omega \frac{d^3N}{dz dL_{\gamma} d\Omega}. \quad (3)$$

Consider a transformation about the normalization, $d^3N/(dz dL_{\gamma} d\Omega) \rightarrow f d^3N/(dz dL_{\gamma} d\Omega)$. By maximizing the likelihood function about f , we find $f = N_{\text{obs}}/N_{\text{exp}}$, i.e., the maximum likelihood obtained when the expected number, fN_{exp} , becomes equal to N_{obs} . Substituting $f = N_{\text{obs}}/N_{\text{exp}}$ and ignoring constant factors that are not relevant for the likelihood maximization, we find the normalization-free form of the likelihood function:

$$\mathcal{L} = \prod_{i=1}^{N_{\text{obs}}} \left(\frac{1}{N_{\text{exp}}} \frac{d^3N(z_i, L_{\gamma,i}, \Omega_i)}{dz dL_{\gamma} d\Omega} \right). \quad (4)$$

The distribution function can be expressed as

$$\begin{aligned} \frac{d^3N}{dz dL_{\gamma} d\Omega} &= \frac{dV}{dz} \rho_{\gamma}(L_{\gamma}, z) \epsilon(L_{\gamma}, z) \\ &\times \Theta[F_{\gamma}(L_{\gamma}, z) - F_{\gamma,\text{lim}}(\Omega)], \end{aligned} \quad (5)$$

where ρ_{γ} is the GLF per unit comoving density and unit luminosity, dV/dz is the comoving volume element per unit solid angle as defined in the standard cosmology, and Θ is the step function [$\Theta(x) = 1$ and 0 for $x \geq 0$ and < 0 , respectively]. The detection efficiency $\epsilon(L_{\gamma}, z)$ represents the identification probability as a blazar by finding a radio counterpart, which will be defined in the next subsection.

To find the best-fit model parameters and their confidence regions, we use the standard likelihood ratio method, assuming that $\mathcal{L} \propto \exp(-\chi^2/2)$, where χ^2 obeys the chi-square distribution. The best-fit parameters are simply obtained as those giving the minimum chi-square, χ^2_{min} , and the confidence region is determined by the contour of a constant $\Delta\chi^2 \equiv \chi^2 - \chi^2_{\text{min}}$. In this paper we will perform two-parameter fit to the data, and hence $\Delta\chi^2$ obeys to the chi-square distribution with two degrees of freedom, i.e., $\Delta\chi^2 = 2.30, 6.16$, and 9.21 for 68%, 95%, and 99% C.L., respectively (see, e.g., Press et al. 1992).

2.3. Identification Probability in Radio Band

Here we formulate the probability that a gamma-ray blazar having a gamma-ray flux above the EGRET detection limit is also detected in the radio band, so that it is identified as an EGRET blazar. In the left panel of Figure 2 we show the observed relation between L_{γ} and radio luminosity L_r (νL_{ν} in erg s⁻¹ at restframe 2.7 GHz) of the EGRET blazars. The

best-fit relation is also shown in the figure (*solid line*). Here we assumed the photon spectral index of $\alpha_r = 1.0$ for the K-correction, as a typical index of blazars in the radio band (Mücke et al. 1997). It should be noted that, though the gamma-ray and radio luminosities are apparently well correlated with each other, this is mostly an artifact, coming from the fact that blazars with different distances are detected with a similar flux around the detection limit. This can easily be understood if we see the correlation plot between observed gamma-ray and radio fluxes, as shown in the right panel of the same figure.

The correlation between gamma-ray and radio emissions of blazars has been investigated and the evidence for this correlation has been presented in many papers (e.g., Padovani et al. 1993; Stecker, Salamon, & Malkan 1993; Salamon & Stecker 1994; Dondi & Ghisellini 1995; Lähteenmäki et al. 1997; Lähteenmäki, Valtaoja, & Tornikoski 2000; Tornikoski & Lähteenmäki 2000; Lähteenmäki & Valtaoja 2001). On the other hand, Mücke et al. (1997) claimed that correlation between the gamma-ray and radio luminosities cannot be established firmly from the existing data. This is probably because the correlation is hidden by intrinsic dispersion and the rather narrow dynamic range of observed radio and gamma-ray fluxes. Based on this result, CM98 assumed no correlation between L_{γ} and L_r .

However, it should be noted that the dynamic range of luminosity of EGRET blazars is extending over more than five order of magnitudes (Fig. 2). If you assume no correlation between gamma-ray and radio luminosities, it means that you cannot tell which blazar is brighter in the radio band, even if you already know that one blazar is brighter than the other by a factor of 10^5 . Such an assumption is highly unlikely, since it is generally believed that the overall spectra of blazars are made by two different emission processes from the same population of relativistic electrons; the gamma-ray emission is due to the inverse Compton process, while the radio emission is due to the synchrotron process. Therefore, we must introduce some correlation between the gamma-ray and radio luminosities in the analysis.

Hence we introduce a linear correlation with log-normal scatter as a simple and phenomenological model, to avoid theoretical uncertainties of more physically motivated models. Then, L_{γ}/L_r obeys to the log-normal distribution with $\langle p \rangle \sim 3.23$, where $p \equiv \log_{10}(L_{\gamma}/L_r)$. Figure 3 shows the distribution of p , and the best-fit dispersion is $\sigma_p = 0.49$. Then, the probability that a blazar having gamma-ray luminosity L_{γ} at redshift z will be identified in radio band can be calculated as the probability that the corresponding radio flux at 2.7 GHz (at observer's frame) is greater than the radio detection limit, $F_{r,\text{lim}}$. We take $F_{r,\text{lim}} = 0.7$ Jy, since most of the EGRET blazars have radio fluxes larger than 0.7 Jy.

It should be noted that this correlation may be different from the true correlation between L_{γ} and L_r , since the observed correlation has been affected by selection effects. The ratio of the flux limits in radio and gamma-ray bands (0.7 Jy at 2.7 GHz and $\sim 1.0 \times 10^{-7}$ photons cm⁻² s⁻¹ above 100 MeV, respectively) is in fact very close to the mean of p . In order to check how much our analysis could be affected by this effect, we calculated the prediction of the p distribution that will actually be observed for the EGRET blazars, from the best-fit models of the blazar GLF that will be obtained later in this paper. We confirmed that the predicted distribution is consistent with the observed one, and this consistency

check demonstrates that our analysis is not seriously biased by the selection effect.

Though we assumed a simple linear relation, more physically motivated models such as the synchrotron self-Compton (SSC) model and the external radiation Compton (ERC) model may predict deviation from the exact linear correlation. However, the above result indicates that the linear correlation is statistically consistent with the data, and we cannot derive more detailed conclusions from the current sample. The future *GLAST* mission may provide better statistics for this issue. We will discuss about the SSC and ERC models in the context of the beaming factor difference in the gamma-ray and radio bands in §5.1.

2.4. Background Photon Flux from Unresolved Blazars

We can calculate the integrated background photon flux (> 100 MeV) from blazars below the EGRET detection limit as

$$F_{\text{diffuse}} = \int_0^{z_{\text{max}}} dz \frac{dV}{dz} \int_{L_{\gamma, \text{min}}}^{L_{\gamma, \text{lim}}(z)} dL_{\gamma} F_{\gamma}(L_{\gamma}, z) \rho_{\gamma}(L_{\gamma}, z), \quad (6)$$

where $L_{\gamma, \text{lim}}(z)$ is the gamma-ray luminosity corresponding to the EGRET threshold, and $L_{\gamma, \text{min}}$ is the minimum gamma-ray luminosity of the blazar GLF. This quantity will be compared with the observed EGRB, to estimate the contribution from unresolved blazars. Since the minimum gamma-ray luminosity is quite uncertain and has considerable effect on the blazar contribution to the EGRB, we consider four values of $L_{\gamma, \text{min}} = 10^{43}, 10^{42}, 10^{41}$, and $10^{40} \text{ erg s}^{-1}$. For reference, $L_{\gamma, \text{min}} = 10^{43} \text{ erg s}^{-1}$ is smaller than the minimum gamma-ray luminosity of the EGRET blazars by a factor of ~ 5 . We assume $z_{\text{max}} = 5$, but the predicted EGRB flux hardly depends on this parameter, since the number density of AGNs with a given luminosity decreases with redshift beyond $z \sim 2$ by the estimated evolution of luminosity functions in the radio or X-ray bands, based on which our GLF models will be constructed.

3. MODELS OF THE BLAZAR GAMMA-RAY LUMINOSITY FUNCTION AND RESULTS OF THE ANALYSIS

In this paper we try two models of the blazar GLF, $\rho_{\gamma}(L_{\gamma}, z)$. The descriptions of these two models and fits to the observed data will be presented below.

3.1. The Pure Luminosity Evolution (PLE) Model

3.1.1. Model Description

For the PLE model, we follow the same procedure proposed by SS96 for constructing the blazar GLF model. They made the basic assumptions that blazars seen by gamma-rays above 100 MeV are also seen in radio as FSRQs, and that the gamma-ray and radio luminosities of these objects are linearly related as

$$L_{\gamma} = 10^{\langle p \rangle} L_r, \quad (7)$$

where the definitions and units are the same as defined in the previous section. The blazar GLF is then derived from the FSRQ RLF:

$$\rho_{\gamma}(L_{\gamma}, z) = \eta \frac{L_r}{L_{\gamma}} \rho_r(L_r, z), \quad (8)$$

where η is a normalization factor, and $\rho_r(L_r, z)$ is the FSRQ RLF. We use the FSRQ RLF derived by Dunlop & Peacock (1990, hereafter DP90):

$$\rho_r(L_r, z) = \frac{1}{f(z)} \rho_r\left(\frac{L_r}{f(z)}, 0\right), \quad (9)$$

where $\rho_r(L_r, 0)$ is the present-day FSRQ RLF, which is characterized by the faint-end slope index γ_1 , the bright-end slope index γ_2 , and the break luminosity L_r^* , given as

$$\rho_r(L_r, 0) = \frac{A_r}{(\ln 10) L_r} \left\{ \left[\frac{L_r}{L_r^*} \right]^{\gamma_1} + \left[\frac{L_r}{L_r^*} \right]^{\gamma_2} \right\}^{-1}, \quad (10)$$

and $f(z)$ is the luminosity evolution function given as

$$f(z) = 10^{az+bz^2}. \quad (11)$$

Here, $A_r = 7.08 \times 10^{-9} \text{ Mpc}^{-3}$, $\log_{10} L_r^* = 42.79$, $\gamma_1 = 0.83$, $\gamma_2 = 1.96$, $a = 1.18$, and $b = -0.28$. Since this FSRQ RLF was derived for the Einstein-de Sitter (EdS) universe with $(\Omega_0, \Omega_{\Lambda}) = (1.0, 0.0)$ and $H_0 = 50 \text{ km s}^{-1} \text{ Mpc}^{-3}$, we multiply $\rho_r(L_r, z)$ by a correction factor $(dV_{\text{EdS}}/dV_{\Lambda})$ and $f(z)$ by a correction factor $(d_{L, \Lambda}/d_{L, \text{EdS}})^2$ in order to approximately convert to a FSRQ RLF for the Λ CDM universe, where dV is the comoving volume element of the universe, and d_L is the luminosity distance. Therefore, this model is no longer ‘‘PLE’’ model in a strict sense, but we take this correction into account to apply the RLF in agreement with the observed data.

3.1.2. Constraints from the Redshift and Luminosity Distribution of the EGRET blazars

In this model, we take $\langle p \rangle$ and γ_1 as the two free parameters since they are poorly constrained from observations, and fix the other parameters to the best-fit values shown in §3.1.1. For consistency, we use the same $\langle p \rangle$ with the dispersion $\sigma_p = 0.49$ also for judgement of the radio identification, which has been described in §2.3. The normalization factor η , which is physically related to the possible beaming effect, is determined by the requirement that the calculated number of identifiable blazars above the EGRET threshold is equivalent to the observed number of the EGRET blazars. In Figure 4 we show the 68%, 95%, and 99% C.L. contours for the PLE model parameters (*solid lines*). The best-fit parameters, $(\langle p \rangle, \gamma_1) = (3.28, 0.69)$, are also marked (*cross*). The value $\langle p \rangle = 3.28$ is quite similar to the value directly obtained from the EGRET blazars ($p = 3.23$). The faint end slope $\gamma_1 = 0.69$ is somewhat smaller (i.e., flatter faint-end slope) than that of the FSRQ RLF derived by DP90 ($\gamma_1 = 0.83$), but the value of DP90 is well within the 68% C.L. region.

Figures 5 and 6 show the redshift and luminosity distributions for the best-fit parameters, respectively (*dashed lines*). It is clear that the PLE model with parameters adopted by SS96 ($\langle p \rangle = 2.54$ and $\gamma_1 = 0.83$ from DP90) can reproduce neither the redshift nor luminosity distributions. Our best-fit model reproduces these distributions better than the SS96 model, but still the fit is not very good, especially for the redshift distribution. We performed the Kolmogorov-Smirnov (KS) test, and find that the chance probability of getting the observed deviation of the redshift distribution from the best-fit PLE model is only 3.1%, while it is 27.0% for the luminosity distribution. These results indicate that the PLE framework may not be satisfactory to describe the EGRET blazar data.

3.1.3. Blazar Contribution to the Extragalactic Diffuse Gamma-Ray Background

In Figure 7 we present the contours of 25%, 50%, 75%, and 100% contribution of blazars under the EGRET sensitivity limit to the EGRB for the PLE model (*dashed lines*). We find that unresolved blazars can explain only 50–55% of the EGRB for the best-fit parameters. On the other hand, since

the contour of 100% blazar contribution pass through inside the 68% C.L. region for all the cases, it is unable to exclude the possibility that almost all of the EGRB is explained by blazars. However, the poor fit of the PLE model to the observed redshift distribution indicates that it is not appropriate to derive any conclusion about the EGRB based on this model framework. It is apparent from this figure that the blazar contribution to the EGRB is strongly dependent on the faint end slope γ_1 . On the other hand, since the EGRB contribution becomes 100% in a region where $\gamma_1 < 1.0$, the minimum gamma-ray luminosity of blazars, $L_{\gamma,\min}$, hardly affects the contribution to the EGRB.

3.2. The Luminosity Dependent Density Evolution (LDDE) Model

3.2.1. Model Description

In this section, we construct the blazar GLF model based on the AGN SXLF by assuming a linear relation between the blazar gamma-ray luminosity (dominated by the jet) and the AGN soft X-ray luminosity (dominated by the disk emission) expressed as

$$L_\gamma = 10^q L_X, \quad (12)$$

where the unit of L_γ (in νL_ν at the restframe 100 MeV) and L_X (in the restframe 0.5–2 keV X-ray band) is erg s^{-1} . In the soft X-ray bands, the typical AGN spectra have a photon index of ~ 2 , i.e., constant in νF_ν , and hence L_X in the observed 0.5–2 keV band is used as that in the restframe 0.5–2 keV band (e.g., Hasinger, Miyaji & Schmidt 2005). The assumption of the linear relation between L_X and L_γ is motivated from an expectation that the jet activity should be somehow correlated with the accretion power which can be measured by X-ray luminosity from accretion disks. It should be noted that this relation is not necessarily be seen in the observed spectral energy distributions of blazars, since X-ray emission from blazars is dominated by the beamed emission from the jet, rather than the disk emission.

The blazar GLF is then obtained from the AGN SXLF:

$$\rho_\gamma(L_\gamma, z) = \kappa \frac{L_X}{L_\gamma} \rho_X(L_X, z), \quad (13)$$

where κ is a normalization factor, and $\rho_X(L_X, z)$ is the AGN SXLF. In this model, we adopt the same form as derived by Hasinger, Miyaji, & Schmidt (2005) for the AGN SXLF, and the details are as follows:

$$\rho_X(L_X, z) = \rho_X(L_X, 0) f(L_X, z), \quad (14)$$

where $\rho_X(L_X, 0)$ is the present-day AGN SXLF, which is characterized by the faint-end slope index γ_1 , the bright-end slope index γ_2 , and the break luminosity L_X^* , given as

$$\rho_X(L_X, 0) = \frac{A_X}{(\ln 10) L_X} \left\{ \left[\frac{L_X}{L_X^*} \right]^{\gamma_1} + \left[\frac{L_X}{L_X^*} \right]^{\gamma_2} \right\}^{-1}, \quad (15)$$

and $f(L_X, z)$ is the density evolution function given as

$$f(L_X, z) = \begin{cases} (1+z)^{p_1} & [z \leq z_c(L_X)] \\ f[L_X, z_c(L_X)] \left[\frac{1+z}{1+z_c(L_X)} \right]^{p_2} & [z > z_c(L_X)] \end{cases}, \quad (16)$$

where z_c is the redshift of evolutionary peak given as

$$z_c(L_X) = \begin{cases} z_c^* & (L_X \geq L_a) \\ z_c^* \left(\frac{L_X}{L_a} \right)^\alpha & (L_X < L_a) \end{cases}, \quad (17)$$

and p_1, p_2 are given as

$$p_1 = p_1^* + \beta_1 (\log_{10} L_X - 44), \quad (18)$$

$$p_2 = p_2^* + \beta_2 (\log_{10} L_X - 44). \quad (19)$$

Here, the parameters obtained by the fit to X-ray data are (Hasinger, Miyaji, & Schmidt 2005): $A_X = 6.69 \times 10^{-7} \text{ Mpc}^{-3}$, $\log_{10} L_X^* = 43.94 \pm 0.11$, $\gamma_1 = 0.87 \pm 0.10$, $\gamma_2 = 2.57 \pm 0.16$, $z_c^* = 1.96 \pm 0.15$, $\log_{10} L_a = 44.67$, $\alpha = 0.21 \pm 0.04$, $p_1^* = 4.7 \pm 0.3$, $p_2^* = -1.5 \pm 0.7$, $\beta_1 = 0.7 \pm 0.3$, and $\beta_2 = 0.6 \pm 0.8$.

3.2.2. Constraints from the Redshift and Luminosity Distribution of the EGRET blazars

In this model, we take q and γ_1 as the two free parameters and fix the rest to the best-fit parameters described in the previous section. For the radio identification judgement, we use the value of $\langle p \rangle = 3.23$ as obtained from the $L_\gamma - L_r$ relation of the EGRET blazars. The normalization factor κ is determined by fitting the expected total number of blazars to the actually observed number of the EGRET blazars. In Figure 8 we show the 68%, 95%, and 99% C.L. contours for the LDDE model (*solid lines*), with the best-fit parameters $(q, \gamma_1) = (3.80, 1.19)$ marked by *cross*. The best-fit value of γ_1 is slightly larger than the value inferred from the SXLF ($\gamma_1 = 0.87 \pm 0.10$), but the SXLF value is within the arrowed region of $\sim 95\%$ confidence level. Figures 5 and 6 show the redshift and luminosity distributions for the best-fit parameters, respectively (*solid lines*). It is noteworthy that the LDDE model can reproduce the redshift and luminosity distributions of the EGRET blazars better than the PLE model. Quantitatively, the chance probability of getting the observed deviation estimated from the KS test is 67.8% and 99.3% for the redshift and luminosity distributions, while these are 3.1% and 27.0% for the best-fit PLE model, respectively. These results indicate that the blazar evolution can better be described by the LDDE rather than the PLE.

3.2.3. Blazar Contribution to the Extragalactic Diffuse Gamma-Ray Background

In Figure 9 we present the contours of 25%, 50%, 75%, and 100% blazar contribution to the EGRB for the LDDE model (*dashed lines*). We find that unresolved blazars can explain only 25–50% of the EGRB for the best-fit parameters. For the case of $L_{\gamma,\min} = 10^{43} \text{ erg s}^{-1}$, the contour of 100% blazar contribution is outside the 99% C.L. region. Still, if we take the case of $L_{\gamma,\min} = 10^{40} \text{ erg s}^{-1}$, the LDDE GLF with $\gamma_1 \sim 1.26$ can marginally explain 100% of the EGRB with the parameters within the 68% C.L. region. However, such a steep faint-end slope index is not favored from the SXLF ($\gamma_1 = 0.87 \pm 0.10$). In the LDDE model the blazar contribution to the EGRB is strongly dependent on the minimum gamma-ray luminosity of blazars $L_{\gamma,\min}$ as well as the faint end slope γ_1 , since the best-fit faint end slope is $\gamma_1 > 1.0$.

4. PREDICTIONS FOR THE GLAST MISSION

4.1. Expected Number of GLAST Blazars and Their Contribution to the EGRB

The number of blazars with flux stronger than F_γ can be calculated as

$$N(> F_\gamma) = 4\pi \int_0^{z_{\max}} dz \frac{dV}{dz} \int_{L_\gamma(z, F_\gamma)}^\infty dL_\gamma \rho_\gamma(L_\gamma, z), \quad (20)$$

where $L_\gamma(z, F_\gamma)$ is the gamma-ray luminosity of a blazar at redshift z whose photon flux above 100 MeV is F_γ (see eq. [1]). In the left panel of Figure 10, we show the calculated $\log N - \log F_\gamma$ relation of blazars. This figure shows that the SS96, our best-fit PLE, and the LDDE models predict considerably different numbers of blazars detectable by the *GLAST* (~ 10000 , 5350 and 3000, respectively), where we have set the *GLAST* sensitivity limit as $F_{\text{lim}} = 2.0 \times 10^{-9}$ photons $\text{cm}^{-2} \text{s}^{-1}$. Here we used $L_{\gamma, \text{min}} = 10^{40}$ erg s^{-1} , but the dependence of the predicted counts on this parameter is small. It is remarkable that the LDDE model predicts more than three times fewer blazars than the SS96 model. This is because the LDDE model predicts smaller evolution for less luminous blazars, and hence paucity of high- z and faint blazars, which have the dominant contribution to the blazar counts at faint flux in the SS96 or our best-fit PLE models. This means that we can constrain different blazar GLF models and their cosmological evolution from the number counts of blazars detected by the *GLAST*, even without knowing their redshifts. We also calculate the predicted counts with the LDDE model parameters of $(q, \gamma_1) = (3.80, 1.26)$, which are within the arrowed region of the 68% C.L. and able to explain 100% of the EGRB. In this case the prediction for the *GLAST* is increased to ~ 4700 , but still smaller than those of the SS96 or the best-fit PLE model.

How much fraction of the EGRB can be resolved by the *GLAST* mission? To answer to this question, in the right panel of Figure 10 we show the differential flux distribution of gamma-ray blazars multiplied by flux, showing the contribution to the EGRB per unit logarithmic flux interval. For the PLE model, we predict that we will see the peak of the contribution to the EGRB above the detection limit of the *GLAST* mission, and hence we will resolve a considerable fraction of the EGRB into blazars, if unresolved blazars are the major source of the EGRB. The predicted resolvable fraction of the EGRB flux by blazars detectable by the *GLAST* (but under the EGRET detection limit) is 33% and 42% for the best-fit PLE model and that with $(\langle p \rangle, \gamma_1) = (3.28, 0.85)$, respectively. The latter model can explain 100% of the EGRB by unresolved blazars. On the other hand, the LDDE model curves have two peaks of the contribution to the EGRB as a function of F_γ , because of the complicated nature of the evolution. We predict that the contribution to the EGRB will decrease with decreasing flux, just below the EGRET sensitivity limit. The resolvable fraction of the EGRB by the *GLAST* is 20% and 26% for the best-fit LDDE model and that with $(q, \gamma_1) = (3.80, 1.26)$, where the latter model can explain 100% of the EGRB. As shown in Figure 10, the dominant contribution to the EGRB comes from blazars under the *GLAST* detection limit, even if blazars are the dominant source of the EGRB.

4.2. Redshift and Luminosity Distribution

In Figures 11 and 12 we show the redshift and luminosity distributions of blazars detectable by the *GLAST*, respectively. It should be noted that only the shapes of distribution should be compared, since the total number has been normalized to the same. It can be seen that the peak of the redshift distribution in the LDDE model occurs at a lower redshift than the best-fit PLE or SS96 models. Furthermore, both redshift and luminosity distributions of the LDDE model are wider than those of the other two models. Though the redshift must be determined for the future *GLAST* blazars, this will provide another important information to discriminate different GLF

models.

5. DISCUSSION

5.1. Normalization, Beaming, and Duty Cycle

In Figures 4 and 8 we also present the contours of η and κ (dashed lines). These parameters are possibly related to a beaming effect and/or duty cycle, and we find $\eta \sim 10^{-0.7}$ and $\kappa \sim 10^{-5.3}$ for the best-fit PLE and LDDE models, respectively. The inferred value of η is not far from the unity, as expected because the GLF was constructed from the luminosity function of FSRQs, which are generally believed to be the same population with blazars. However, the best-fit value $\eta \sim 10^{-0.7}$ is slightly smaller than the unity. In the SSC model, this value may be explained if not all FSRQs are sufficiently gamma-ray-loud, or there are more than one components of nonthermal electrons or emission regions having different beaming patterns (e.g., Lindfors et al. 2005). On the other hand, the ERC model may explain this value of η by a single electron component, since the beaming pattern of the ERC emission is narrower than that of the synchrotron emission or the SSC emission (Dermer 1995). The observed flux has an angular dependence $S_\nu \propto \mathcal{D}^{2+\alpha}$ for the synchrotron or SSC processes, and $S_\nu \propto \mathcal{D}^{2+2\alpha}$ for the ERC process, where \mathcal{D} is the Doppler factor and α is the photon spectral index. Here we define θ_e as the viewing angle of the observer measured from the jet axis, at which the observed flux is smaller than that for the direction of the jet axis by a factor of e . Then, using the Lorentz factor $\Gamma = 10$ and the typical index ($\alpha_\gamma = 2.2$, $\alpha_r = 1.0$), we find that $\theta_e \sim 3.6^\circ$ for the synchrotron emission, while $\theta_e \sim 2.1^\circ$ for the ERC emission. Therefore $\eta \sim (2.1/3.6)^2 \sim 0.34$ is expected in this case, which is moderately close to $\eta \sim 10^{-0.7}$.

On the other hand, the GLF in the LDDE model is constructed from that of AGNs selected in the soft X-ray band, most of which are expected to be type 1 AGNs. Since the jet activity is not always observed in AGNs, it is rather unlikely that all X-ray AGNs have blazar activity. Then, the interpretation of the small value of κ is a combination of the duty cycle ξ (here defined as the fraction of AGNs having the blazar activity) and beaming of radiation, i.e.,

$$\kappa = \frac{\xi}{f_{\text{type1}}} \frac{\Delta\Omega}{4\pi} \quad (21)$$

$$= 5 \times 10^{-6} \left(\frac{f_{\text{type1}}}{0.2} \right)^{-1} \left(\frac{\Delta\Omega/(4\pi)}{10^{-3}} \right) \left(\frac{\xi}{10^{-3}} \right). \quad (22)$$

Here, we take the ratio of SXLF to HXLF normalization as the fraction of type 1 AGNs in all AGNs, f_{type1} (Hasinger, Miyaji, & Schmidt 2005). The beaming expected from the estimated Lorentz factor of blazars ($\Gamma \sim 10$ –20, e.g., Maraschi & Tevetchio 2003) is $\Delta\Omega/(4\pi) \sim 1/(4\Gamma^2) \sim 10^{-3}$. The small duty cycle can partially be ascribed to the fraction of radio-loud AGNs to all AGNs, $f_{\text{radio}} \sim 0.15$ (Urry & Padovani 1995; Krolik 1999). Comparing this f_{radio} to the inferred ξ , it is indicated that about 1% of radio-loud galaxies have active jets now. It is not unreasonable, since the jet activity may be sporadic, and radio emission by relic electrons can be kept for a while after the jet activity ceased.

5.2. Unidentified EGRET Sources

Over half of the gamma-ray sources (170 of 271) detected by the EGRET have not been identified as known astronomical objects. The distribution of these unidentified sources

can be accounted for as the sum of the Galactic and another isotropic (likely extragalactic) component (Mukherjee et al. 1995; Özel & Thompson 1996). Since most of the firmly identified extragalactic sources are blazars, it is widely believed that many of the unidentified extragalactic sources which show high variability are blazars. Actually, many researchers have been investigating the unidentified EGRET sources in various wavelengths to find their counterparts, and some of them, such as 3EG J2016+3657 (Mukherjee et al. 2000; Halpern et al. 2001), 3EG J2006-2321 (Wallace et al. 2002), and 3EG J2027+3429 (Sguera et al. 2004), have already been identified as blazars. In addition, the number of blazar candidates in the unidentified sources is now increasing (e.g., Sowards-Emmerd, Romani, & Michelson 2003; Bloom et al. 2004; Wallace, Bloom, & Lewis 2005).

These (potential) blazars were initially classified as unidentified sources likely because of the lack of strong radio emission. Since our model incorporates the dispersion in radio and gamma-ray luminosities and selection by radio flux, we can address this issue by estimating how many “unidentified blazars” will be expected due to the lack of detectable radio flux. We found that this number is 10 and 8 sources at high Galactic latitude of $|b| > 45^\circ$ for the best-fit PLE and LDDE models, respectively². In the third EGRET catalog, there are six low confidence potential blazars and 19 unidentified sources at $|b| > 45^\circ$. The variability of these unidentified sources have been investigated in some papers (e.g., Gehrels et al. 2000; Torres, Pessah, & Romero 2001; Nolan et al. 2003), and 5–9 of them are non-variable sources, though definition of “non-variable” is different among these papers. Therefore, a substantial fraction of potential blazars and variable unidentified sources at $|b| > 45^\circ$ can be explained by blazars with radio flux under the detection limit. It has been suggested that the apparently steady unidentified sources may be accounted for by forming gamma-ray clusters (Totani & Kitayama 2000).

6. CONCLUSIONS

In this paper, we presented a comprehensive study for the gamma-ray luminosity function of blazars. We introduced a log-normal distribution for the ratio of radio to gamma-ray luminosity, and radio detection was required for the model blazars to become identified sources in the EGRET catalog. The number of potential blazars and variable unidentified sources at high Galactic latitude in the EGRET catalog is similar to the number of “unidentified blazars” predicted in our model due to the lack of detectable radio flux, indicating that our treatment about gamma-ray blazar identification by radio detection is reasonable. We newly tried the luminosity dependent density evolution (LDDE) model based on recent studies of the X-ray luminosity function of AGNs, in addition to the pure luminosity evolution (PLE) model used in earlier studies.

By performing the maximum likelihood analysis for the redshift and luminosity distributions of the EGRET blazars, we found that the LDDE model with the evolutionary parameters inferred from the soft X-ray luminosity function (SXLF) of AGNs can explain the redshift and luminosity distributions of the EGRET blazars better than the PLE model with the evolutionary parameters inferred from the radio luminosity function (RLF) of flat-spectrum radio-loud quasars (FSRQs). This indicates that blazars are evolving similarly to type 1 AGNs

found in the soft X-ray bands, and hence the jet activity is universally correlated with the accretion history of AGNs. We also found that the normalization between blazars and type 1 AGNs is roughly consistent with the unified picture of AGNs, when the beaming and jet duty cycle are taken into account.

As an implication for the *GLAST* mission, we found that the LDDE model predicts considerably fewer (by a factor of more than 3) blazars down to the *GLAST* sensitivity limit, compared with a previous estimate based on the PLE luminosity function. This can be easily tested by the mission, giving us important information for the evolutionary nature of gamma-ray blazars. Redshift and luminosity distributions will further constrain the different models, though redshift measurements are required.

Then we examined the contribution of unresolved blazars to the extragalactic diffuse gamma-ray background (EGRB), which has been controversial topic in earlier works (100% in SS96, 25% in CM98). We found that only 25–50% of the EGRB can be explained with the best-fit LDDE model, which is similar to the result of CM98 but by considerably different analysis. On the other hand, according to our statistical analysis and parameter survey, it is possible to account for 100% of the EGRB with a steeper faint-end slope of $\gamma_1 \sim 1.26$ that is marginally consistent with the arrowed region from the likelihood analysis of the EGRET blazar distributions. However, such a value is inconsistent with that inferred from the SXLF of AGNs. Therefore we conclude that unresolved blazars cannot account for 100% of the EGRB, if the jet activity of AGNs is universally correlated to the accretion luminosity and hence the AGN SXLF is a good description of the blazar luminosity function and its evolution. It should be noted that the uncertainty about the extrapolation to high redshift does not change this conclusion, since almost all of the cosmic X-ray background (CXB) flux can be explained by the LDDE luminosity function (Ueda et al. 2003). It indicates that, if the rest of the EGRB is explained by an AGN population, it must be a different population from EGRET blazars, having different evolution from X-ray AGNs, and not significantly contributing to the CXB.

Based on the best-fit LDDE model, we predict that the contribution to the EGRB by blazars will start to decrease with decreasing flux just below the EGRET sensitivity limit. In the case of the LDDE model with parameters that can explain 100% of the EGRB, there are two peaks of the contribution to the EGRB as a function of flux, and the major contribution comes from blazars under the *GLAST* detection limit. Therefore it is unlikely that almost all the EGRB flux is resolved into discrete blazars even by the sensitivity of *GLAST*.

This work was supported by the Grant-in-Aid for the 21st Century COE “Center for Diversity and Universality in Physics” from the Ministry of Education, Culture, Sports, Science and Technology (MEXT) of Japan.

² The Galactic component of unidentified sources extends only to $|b| \sim 45^\circ$ (Gehrels et al. 2000).

REFERENCES

- Bloom, S. D., et al. 2004, *ApJ*, 128, 56
- Boyle, B. J., Georgantopoulos, I., Blair, A. J., Stewart, G. C., Griffiths, R. E., Shanks, T., Gunn, K. F., & Almaini, O. 1998, *MNRAS*, 296, 1
- Chiang, J., Fichtel, C. E., von Montigny, C., Nolan, P. L., & Petrosian, V. 1995, *ApJ*, 452, 156
- Chiang, J., & Mukherjee, R. 1998, *ApJ*, 496, 752 (CM98)
- Cowie, L. L., Barger, A. J., Bautz, M. W., Brandt, W. N., & Garmire, G. P. 2003, *ApJ*, 584, L57
- Dermer, C. D. 1995, *ApJ*, 446, L63
- Dondi, L., & Ghisellini, G. 1995, *MNRAS*, 273, 583
- Dunlop, J. S., & Peacock, J. A. 1990, *MNRAS*, 247, 19 (DP90)
- Fichtel, C. E., Simpson, G. A., & Thompson, D. J. 1978, *ApJ*, 222, 833
- Gabici, S., & Blasi, P. 2003, *Astrophys. J.*, 19, 679
- Gehrels, N., Macomb, D. J., Bertsch, D. L., Thompson, D. J., & Hartman, R. C. 2000, *Nature*, 404, 363
- Halpern, J. P., Eracleous, M., Mukherjee, R., & Gotthelf, E. V. 2001, *ApJ*, 551, 1016
- Hartman, R. C., et al. 1999, *ApJS*, 123, 79
- Hasinger, G., Miyaji, T., & Schmidt, M. 2005, *A&A*, 441, 417
- Keshet, U., Waxman, E., Loeb, A., Springel, V., & Hernquist, L. 2003, *ApJ*, 585, 128
- Krolik, J. H. 1999, *ACTIVE GALACTIC NUCLEI: From the Central Black Hole to the Galactic Environment* (Princeton: Princeton Univ. Press)
- La Franca, F., et al. 2002, *ApJ*, 570, 100
- Lähteenmäki, A., Teräsranta, H., Wiik, K., & Valtaoja, E. 1997, in 4th Compton Symposium on Gamma-Ray Astronomy and Astrophysics, ed. C. D. Dermer, M. S. Strickman, & J. D. Kurfess (New York: AIP), 1452
- Lähteenmäki, A., & Valtaoja, E. 2001, in *Gamma 2001*, ed. S. Ritz, N. Gehrels, & C. R. Shrader (New York: AIP), 301
- Lähteenmäki, A., Valtaoja, E., & Tornikoski, M. 2000, in 5th Compton Symposium on Gamma-Ray Astronomy and Astrophysics, ed. M. L. McConnell & J. M. Ryan (New York: AIP), 372
- Lindfors, E. J., Valtaoja, E., Türler, M. 2005, *A&A*, 440, 845
- Loeb, A., & Waxman, E. 2000, *Nature*, 405, 156
- Lored, T. J., & Lamb, D. Q. 1989, *Annals New York Academy of Sciences*, 571, 601
- Maraschi, L., & Tavecchio, F. 2003, *ApJ*, 593, 667
- Miniati, F. 2002, *MNRAS*, 337, 199
- Miyaji, T., Hasinger, G., & Schmidt, M. 2000, *A&A*, 353, 25
- . 2001, *A&A*, 369, 49
- Mücke, A., & Pohl, M. 2000, *MNRAS*, 312, 177
- Mücke, A., et al. 1997, *A&A*, 320, 33
- Mukherjee, R., Bertsch, D. L., Dingus, B. L., Kanbach, G., Kniffen, D. A., Sreekumar, P., & Thompson, D. J. 1995, *ApJ*, 441, L61
- Mukherjee, R., Gotthelf, E. V., Halpern, J., & Tavani, M. 2000, *ApJ*, 542, 740
- Nolan, P. L., Tompkins, W. F., Grenier, I. A., & Michelson, P. F. 2003, *ApJ*, 597, 615
- Oda, T., Totani, T., & Nagashima, M. 2005, *ApJ*, 633, L65
- Özel, M. E., & Thompson, D. J. 1996, *ApJ*, 463, 105
- Padovani, P., Ghisellini, G., Fabian, A. C., & Celotti, A. 1993, *MNRAS*, 260, L21
- Press, W. H., Teukolsky, S. A., Vetterling, W. T., & Flannery, B. P. 1992, *Numerical Recipes in C* (Cambridge: Cambridge Univ. Press)
- Salamon, M. H., & Stecker, F. W. 1994, *ApJ*, 430, L21
- Scharf, C. A., & Mukherjee, R. 2002, *ApJ*, 580, 154
- Sguera, V., Malizia, A., Bassani, L., Stephen, J. B., & Di Cocco, G. 2004, *A&A*, 414, 839
- Sowards-Emmerd, D., Romani, R. W., & Michelson, P. F. 2003, *ApJ*, 590, 109
- Sreekumar, P., et al. 1998, *ApJ*, 494, 523
- Stecker, F. W., & Salamon, M. H. 1996, *ApJ*, 464, 600 (SS96)
- . 2001, preprint (astro-ph/0104368)
- Stecker, F. W., Salamon, M. H., & Malkan, M. A. 1993, *ApJ*, 410, L71
- Strong, A. W., Moskalenko, I. V., & Reimer, O. 2004, *ApJ*, 613, 956
- Thompson, D. J., & Fichtel, C. E. 1982, *A&A*, 109, 352
- Tornikoski, M., & Lähteenmäki, A. 2000, in 5th Compton Symposium on Gamma-Ray Astronomy and Astrophysics, ed. M. L. McConnell & J. M. Ryan (New York: AIP), 377
- Torres, D. F., Pessah, M. E., & Romero, G. E. 2001, *Astron. Nachr.*, 322, 223
- Totani, T., Kitayama, T. 2000, *ApJ*, 545, 572
- Ueda, Y., Akiyama, M., Ohta, K., & Miyaji, T. 2003, *ApJ*, 598, 886
- Urry, C. M., & Padovani, P. 1995, *PASP*, 107, 803
- Wallace, P., Bloom, S., & Lewis, M. 2005, *Ap&SS*, 297, 409
- Wallace, P. M., Halpern, J. P., Magalães, A. M., & Thompson, D. J. 2002, *ApJ*, 569, 36

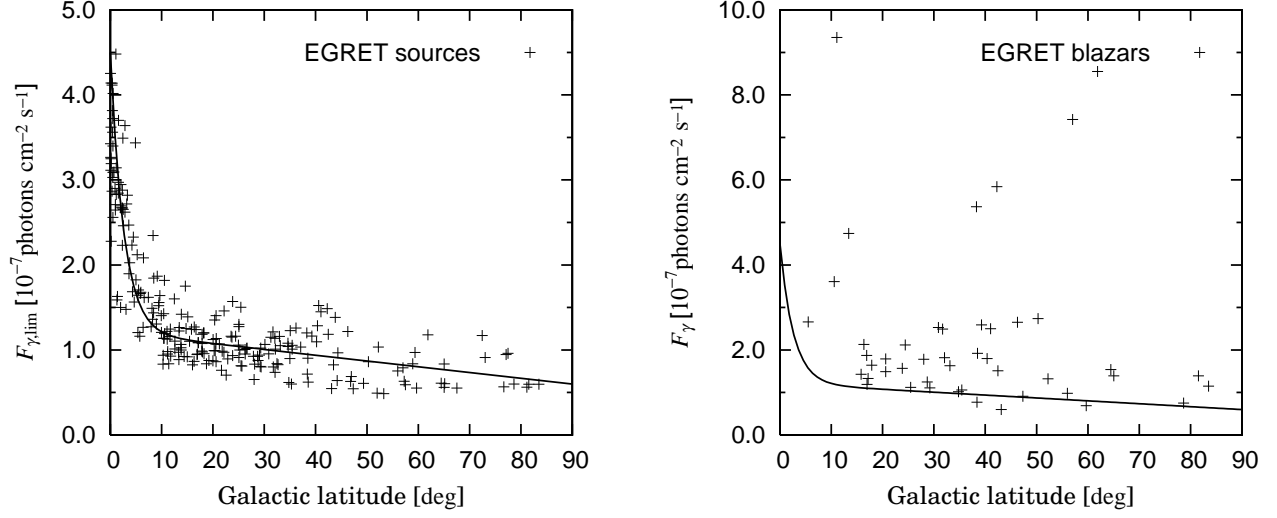


FIG. 1.— Left panel: Sensitivity limit to point sources as a function of the Galactic latitude in the third EGRET catalog. The fitted relation is also shown by the solid line. Right panel: mean flux of the EGRET blazars against its Galactic latitude. The solid line is the same as the left panel.

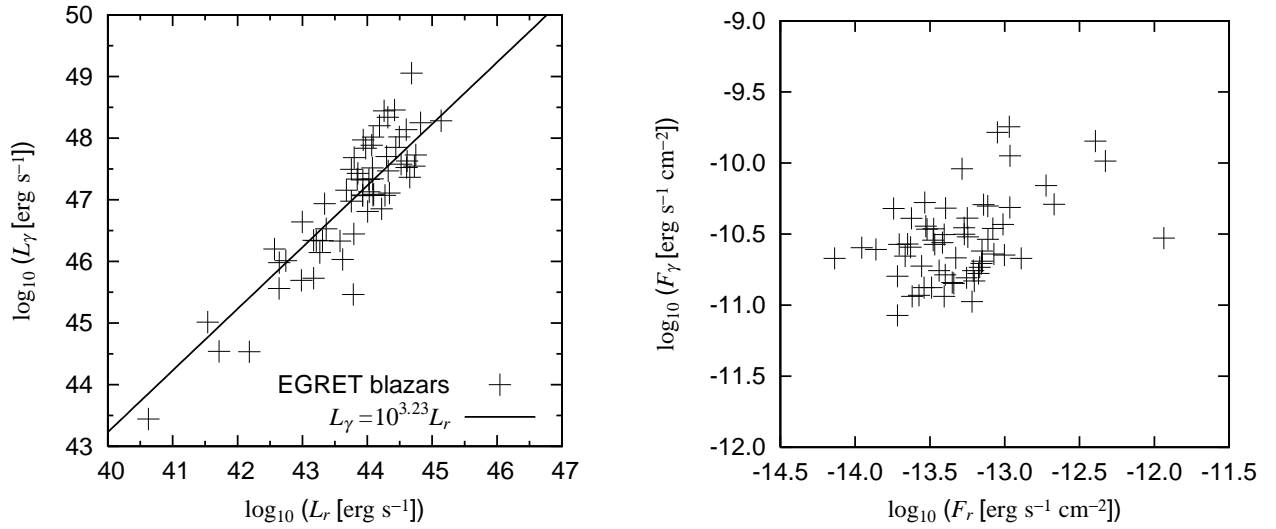


FIG. 2.— Left (Right) panel: Observed gamma-ray and radio luminosities (fluxes) of the EGRET blazars are shown by the crosses. Here, the luminosity (flux) is defined as νL_{ν} (νF_{ν}) at restframe (observed) 100 MeV and 2.7 GHz for the gamma-ray and radio bands, respectively. The solid line is the best-fit linear relation. The K-corrections are done for luminosities assuming typical spectral indices (see text).

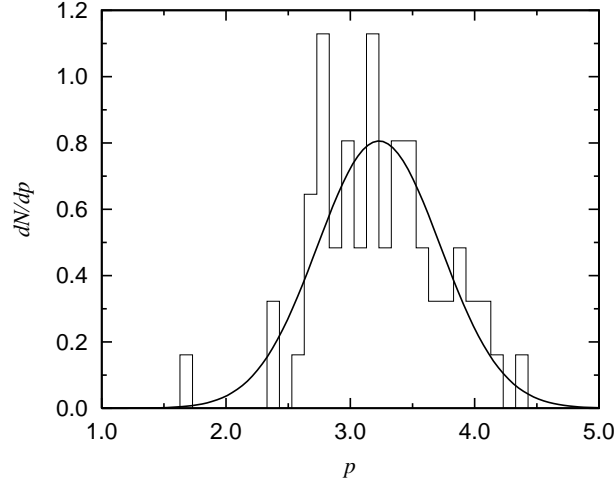


FIG. 3.— Histogram of radio to gamma-ray luminosity ratio, $p = \log_{10}(L_{\gamma}/L_r)$, of the EGRET blazars. The luminosities are νL_{ν} in the restframe 100 MeV and 2.7 GHz bands, respectively. The solid curve is a Gaussian fit to the histogram.

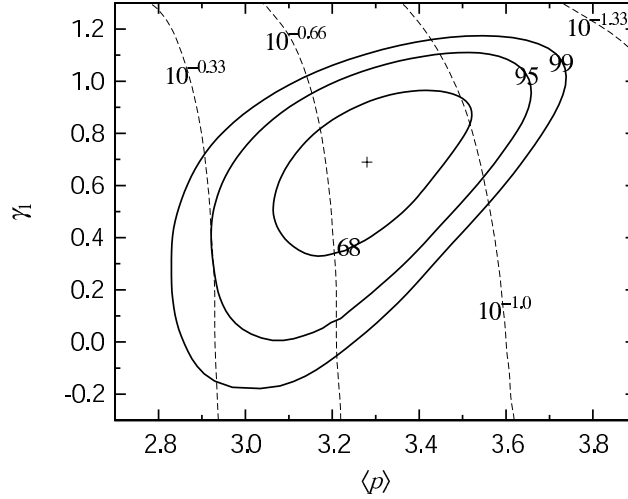


FIG. 4.— The solid contours show the 68%, 95% and 99% C.L. regions for the PLE model parameters [the faint-end slope index γ_1 and the mean gamma-ray to radio luminosity ratio, $\langle p \rangle = \langle \log_{10}(L_{\gamma}/L_r) \rangle$]. The best-fit values, $(\langle p \rangle, \gamma_1) = (3.28, 0.69)$, are shown by the cross. The dashed contours correspond to $\eta = 10^{-0.33}$, $10^{-0.66}$, $10^{-1.0}$, and $10^{-1.33}$, respectively, where η is the ratio of the normalizations of the gamma-ray to radio luminosity functions.

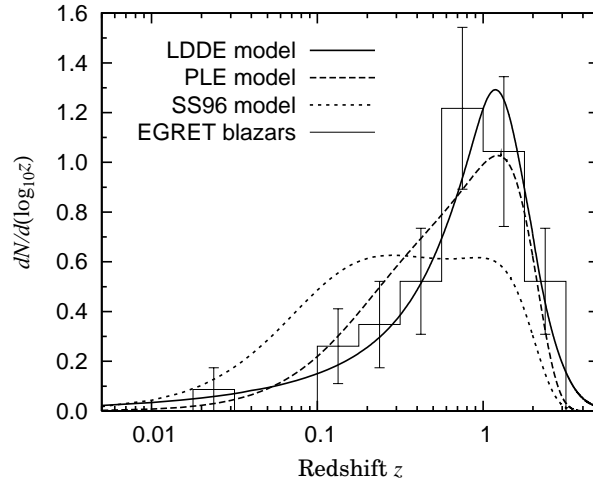


FIG. 5.— Redshift distribution of the EGRET blazars. The histogram is the EGRET data. The solid and dashed curves are the best-fit models for the LDDE and PLE models, respectively, from the likelihood analysis. The dotted curve is obtained from the blazar GLF model of SS96. The error bars are 1σ Poisson error.

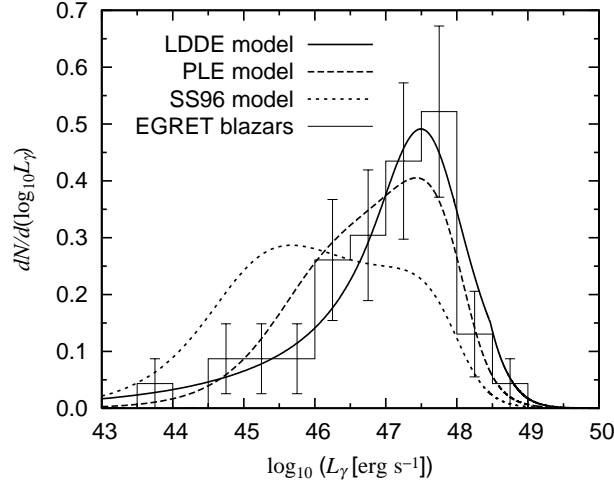


FIG. 6.— Luminosity distribution of the EGRET blazars. The line markings are the same as Figure 5. The luminosity is νL_ν at 100 MeV. The error bars are 1σ Poisson error.

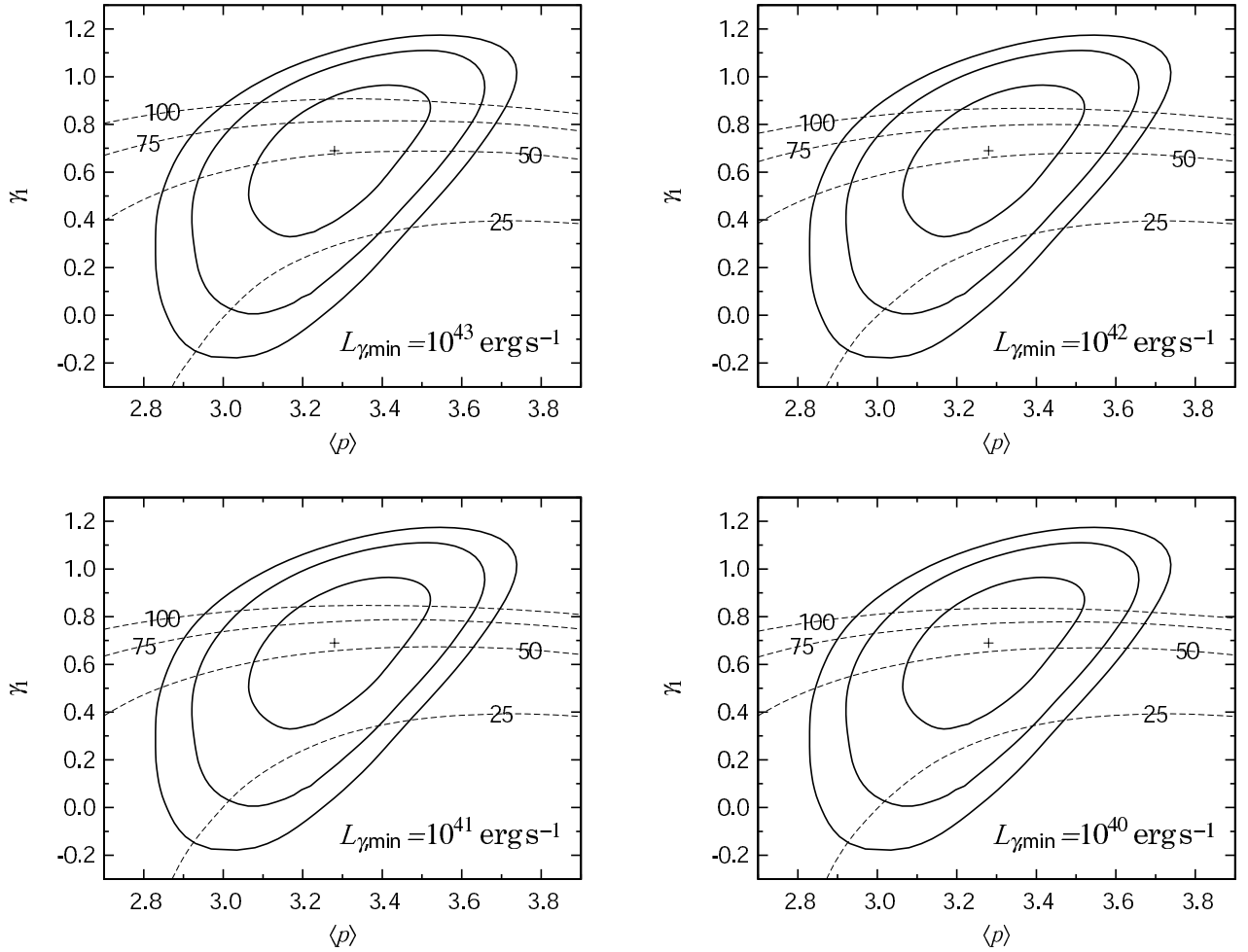


FIG. 7.— The solid contours and crosses are the same as Figure 4 showing the fit by the PLE model. The dashed contours show 25%, 50%, 75%, and 100% contribution of unresolved blazars to the EGRB. The upper left, upper right, lower left, and lower right panels are for the cases of $L_{\gamma,\min} = 10^{43}$, 10^{42} , 10^{41} , and 10^{40} erg s $^{-1}$, respectively.

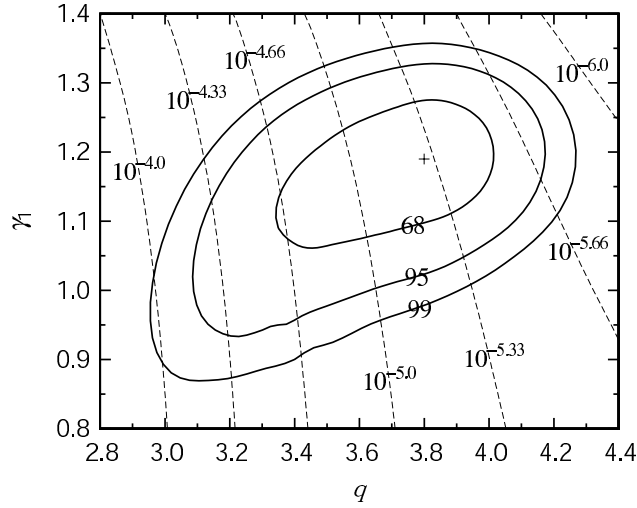


FIG. 8.— The solid contours show the 68%, 95% and 99% C.L. likelihood contours for the LDDE model parameters [the faint-end slope index γ_1 and the gamma-ray to X-ray luminosity ratio, $q \equiv \log_{10}(L_\gamma/L_X)$]. The best-fit values, $(q, \gamma_1) = (3.80, 1.19)$, are shown by the cross. The dashed contours correspond to $\kappa = 10^{-4.0}, 10^{-4.33}, 10^{-4.66}, 10^{-5.0}, 10^{-5.33}, 10^{-5.66}$, and $10^{-6.0}$, respectively, where κ is the normalization ratio of the gamma-ray to soft X-ray luminosity functions.

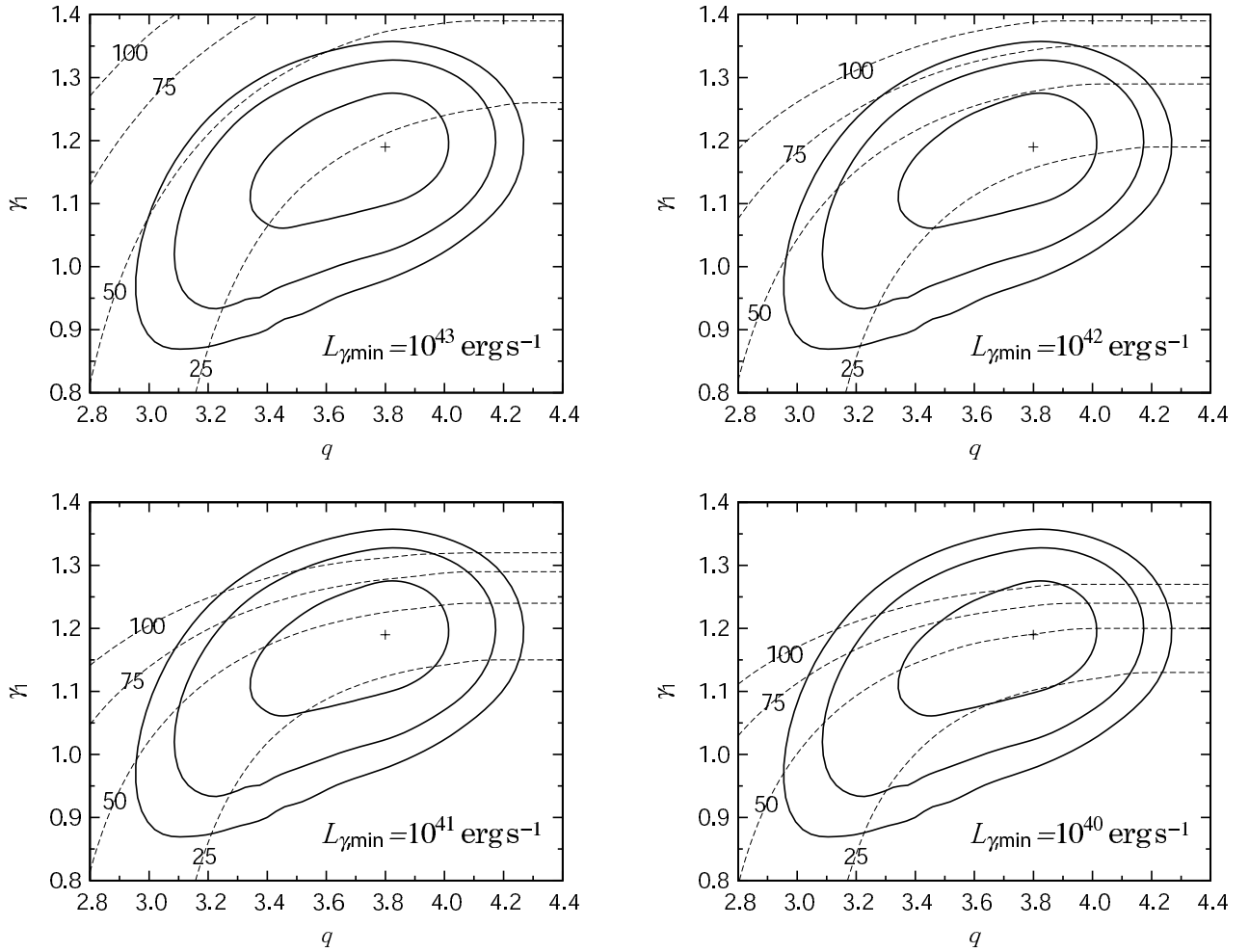


FIG. 9.— The solid contours and crosses are the same as Figure 8, showing the fit by the LDDE model. The dashed contours show 25%, 50%, 75%, and 100% contribution of unresolved blazars to the EGRB. The upper left, upper right, lower left, and lower right panels are for the cases of $L_{\gamma,\min} = 10^{43}, 10^{42}, 10^{41}$, and $10^{40} \text{ erg s}^{-1}$, respectively.

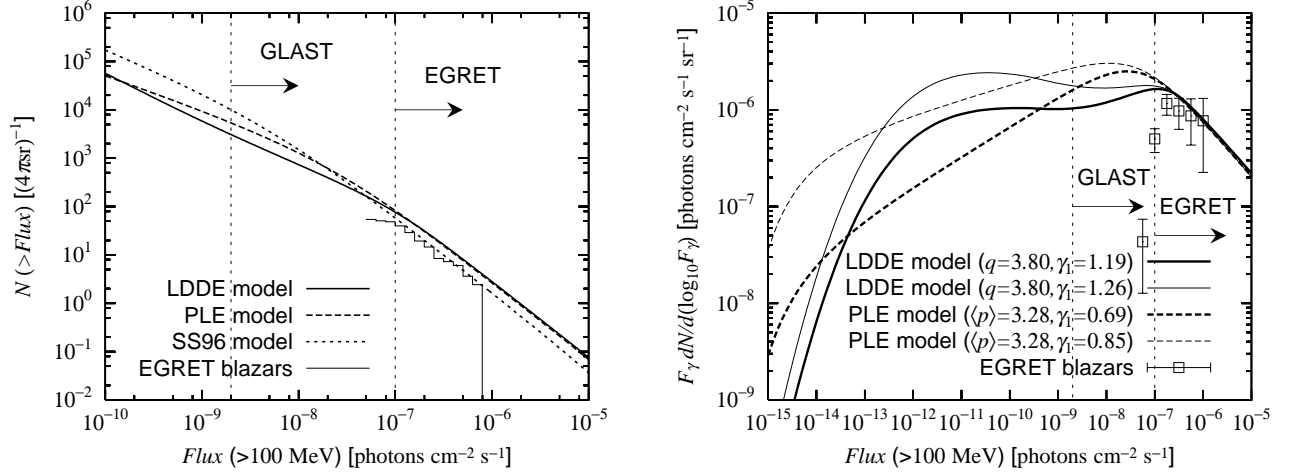


FIG. 10.— Left panel: $\log N - \log F$ distribution (cumulative flux distribution) of blazars. The solid and dashed curves show the prediction by the best-fit LDDE and PLE models, respectively. The dotted curve is derived from the blazar GLF model of SS96. The observed distribution of the EGRET blazars is shown by the thin solid line. The detection limits of the EGRET and *GLAST* are also shown in the figure. Right panel: The same as the left panel, but showing differential flux distribution multiplied by F_γ , to show the contribution to the EGRB per logarithmic flux interval. The thick solid and dashed curves are the same as those in the left panel, but the thin solid and dashed curves show the LDDE and PLE models with parameters that can explain all the EGRB flux by unresolved blazars. (See the labels in the panel for the values of the parameters.)

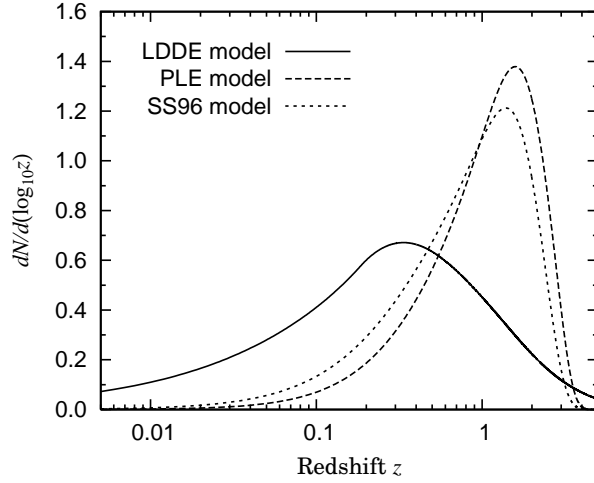


FIG. 11.— Redshift distribution of blazars expected for the *GLAST* observation. The total number is normalized to the same. The solid and dashed curves show the prediction by the best-fit LDDE and PLE models, respectively. The dotted curve is predicted from the blazar GLF model of SS96. The *GLAST* sensitivity limit is set as $F_{\text{lim}} = 2.0 \times 10^{-9} \text{ photons cm}^{-2} \text{ s}^{-1}$.

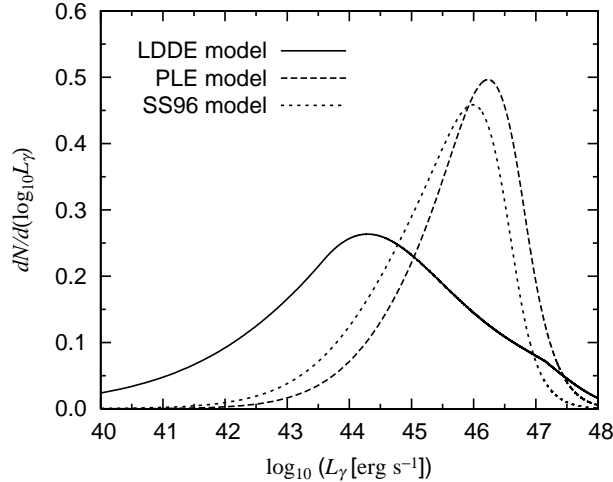


FIG. 12.— Luminosity distribution of blazars expected for the *GLAST* observation. The total number is normalized to the same. The line markings are the same as Figure 11. The *GLAST* sensitivity limit is set as $F_{\text{lim}} = 2.0 \times 10^{-9} \text{ photons cm}^{-2} \text{ s}^{-1}$.